Neurobiology of Learning and Memory 171 (2020) 107207

Contents lists available at ScienceDirect

Neurobiology of Learning and Memory

journal homepage: www.elsevier.com/locate/ynlme

Long-term changes in metabolic brain network drive memory impairments in rats following neonatal hypoxia-ischemia

Pamella Nunes Azevedo[a,c], Gabriele Zanirati[b,c], Gianina Teribele Venturin[d], Guilherme Garcia Schu[e], Luz Elena Durán–Carabali[e], Felipe Kawa Odorcyk[e], Andrey Vinicius Soares[e], Gabriela de Oliveira Laguna[b], Carlos Alexandre Netto[e], Eduardo Rigon Zimmer[e,f,g,h], Jaderson Costa da Costa[a,b,c,d], Samuel Greggio[d,*]

[a] Graduate Program in Medicine and Health Sciences School of Medicine, Pontifical Catholic University of Rio Grande do Sul (PUCRS), Porto Alegre, Brazil
[b] Graduate Program in Pediatrics and Child Health, School of Medicine, Pontifical Catholic University of Rio Grande do Sul (PUCRS), Porto Alegre, Brazil
[c] Laboratory of Neuroscience Brain Institute (BraIns) of Rio Grande do Sul, Porto Alegre, Brazil
[d] Preclinical Research Center, Brain Institute (BraIns) of Rio Grande do Sul, Porto Alegre, Brazil
[e] Department of Biochemistry Federal University of Rio Grande do Sul (UFRGS), Porto Alegre, Brazil
[f] Department of Pharmacology Federal University of Rio Grande do Sul (UFRGS), Porto Alegre, Brazil
[g] Graduate Program in Biological Sciences: Biochemistry Federal University of Rio Grande do Sul (UFRGS), Porto Alegre, Brazil
[h] Graduate Program in Biological Sciences: Pharmacology and Therapeutics, Federal University of Rio Grande do Sul (UFRGS), Porto Alegre, Brazil

ARTICLE INFO

Keywords:
Neuronal plasticity
microPET
^{18}F-FDG
Neonatal hypoxia ischemia
Metabolic brain network

ABSTRACT

Background and purpose: Hypoxia and cerebral ischemia (HI) events are capable of triggering important changes in brain metabolism, including glucose metabolism abnormalities, which may be related to the severity of the insult. Using positron emission microtomography (microPET) with [^{18}F]fluorodeoxyglucose (^{18}F-FDG), this study proposes to assess abnormalities of brain glucose metabolism in adult rats previously submitted to the neonatal HI model. We hypothesize that cerebral metabolic outcomes will be associated with cognitive deficits and magnitude of brain injury.

Methods: Seven-day-old rats were subjected to an HI model, induced by permanent occlusion of the right common carotid artery and systemic hypoxia. ^{18}F-FDG-microPET was used to assess regional and whole brain glucose metabolism in rats at 60 postnatal days (PND 60). An interregional cross-correlation matrix was utilized to construct metabolic brain networks (MBN). Rats were also subjected to the Morris Water Maze (MWM) to evaluate spatial memory and their brains were processed for volumetric evaluation.

Results: Brain glucose metabolism changes were observed in adult rats after neonatal HI insult, limited to the right brain hemisphere. However, not all HI animals exhibited significant cerebral hypometabolism. Hippocampal glucose metabolism was used to stratify HI animals into HI hypometabolic (HI-h) and HI non-hypometabolic (HI non-h) groups. The HI-h group had drastic MBN disturbance, cognitive deficit, and brain tissue loss, concomitantly. Conversely, HI non-h rats had normal brain glucose metabolism and brain tissue preserved, but also presented MBN changes and spatial memory impairment. Furthermore, data showed that brain glucose metabolism correlated with cognitive deficits and brain volume outcomes.

Conclusions: Our findings demonstrated that long-term changes in MBN drive memory impairments in adult rats subjected to neonatal hypoxic ischemia, using *in vivo* imaging microPET-FDG. The MBN analyses identified glucose metabolism abnormalities in HI non-h animals, which were not detected by conventional ^{18}F-FDG standardized uptake value (SUVr) measurements. These animals exhibited a metabolic brain signature that may explain the cognitive deficit even with no identifiable brain damage.

* Corresponding author at: Preclinical Research Center, Brain Institute of Rio Grande do Sul (BraIns), Pontifical Catholic University of Rio Grande do Sul (PUCRS), Avenida Ipiranga 6690, Jardim Botânico, Prédio 63, sala 140, CEP 90610-000 Porto Alegre, RS, Brazil.
E-mail address: samuel.greggio@pucrs.br (S. Greggio).

https://doi.org/10.1016/j.nlm.2020.107207
Received 6 November 2019; Received in revised form 13 February 2020; Accepted 2 March 2020
Available online 05 March 2020

1. Introduction

Neonatal hypoxic-ischemic encephalopathy (HI) is the most common cause of mortality and chronic neurological morbidity in infants. HI affects about 26 out of every 1000 live births, leading to permanent neurological disabilities (Kurinczuk, White-Koning, & Badawi, 2010). Despite considerable advances in neonatal care, clinical management of asphyxiated children is limited to supportive measures and there are few options for preventing or interrupting brain injury mechanisms (Johnston, Fatemi, Wilson, & Northington, 2011; Shankaran, 2012).

In this scenario, experimental models are important tools for investigation of new approaches to obtaining better understanding of the pathophysiological features of children affected by HI. The Rice-Vannucci HI rodent model mimics multiple injury mechanisms and neurological impairments that are reported in affected children (Rice, Vannucci, & Brierley, 1981). In humans and in animal models, the severity and distribution of neuropathological injuries are directly related to factors such as duration of insult, age, and genetic background. Despite the controlled conditions for induction of HI in rodents, the literature contains divergent descriptions of the extent of brain damage and also of presence or absence of motor and cognitive impairments (De Paula et al., 2009; Durán-Carabali et al., 2017; Lubics et al., 2005; Millar, Shi, Hoerder-Suabedissen, & Molnár, 2017; Netto, Sanches, Odorcyk, Duran-Carabali, & Weis, 2017; Sanches, Arteni, Nicola, Aristimunha, & Netto, 2015). These discrepancies have been attributed to the neuroplasticity of the immature brain leading to spontaneous recovery (Jung et al., 2016).

The main mechanisms attributed to neonatal HI neuropathology are reduced supply of oxygen or glucose to the brain tissue. Drastic reduction of cerebral blood flow leads to a cascade of irreversible harmful effects in the newborn brain (Brekke et al., 2014; McKenna, Scafidi, & Robertson, 2015). Cerebral metabolic changes associated with HI brain injury have been reported in animal models of neonatal HI (Malisza, Kozlowski, Ning, Bascaramurty, & Tuor, 1999; Sanches et al., 2018; Vial et al., 2004). In this context, high-resolution small-animal positron emission microtomography (microPET), with [^{18}F]fluorodeoxyglucose (^{18}F-FDG), provides an interesting tool to investigate *in vivo* changes in brain glucose metabolism in the HI model. Here, we aimed to evaluate whether neonatal HI causes persistent changes to brain glucose metabolism in adult rats and whether these changes are associated with behavioral and histological outcomes.

2. Material and methods

2.1. Animals

All experimental procedures were performed with the approval of the Animal Care and Ethics Committee at the Federal University of Rio Grande do Sul (UFRGS), Rio Grande do Sul, Brazil (Protocol number: 31939). All experimental practices comply with international standards for experimentation with laboratory animals and were carried out taking all necessary measures to reduce to the minimum the number of animals used and their suffering. Male Wistar rats were used for the experimental procedures despite the higher vulnerability to HI insult. The litters were standardized to 8–10 neonate rats and kept in standard cages, under controlled environmental conditions – temperature of 23 °C ± 1 °C and 12 h dark-light cycle with food and water *ad libitum*. Thirty-four rats were randomly allocated to the experimental groups: control group (sham, n = 12) and hypoxic-ischemic group (HI, n = 22). The day of birth was considered postnatal day zero (PND 0).

2.2. Neonatal hypoxia-ischemia model

The HI model used in the present study was first described by Levine (1960) and modified by Rice et al. (1981). Seven day-old Wistar rats were anesthetized with isoflurane (3–4% for induction and 2–3% for maintenance) and the right common carotid artery was permanently occluded with 4.0 surgical silk threads. After total recovery from anesthesia, the animals were returned to their home cages for a feeding period for 2 h. At the end of this period, pups were exposed to a hypoxic environment (8% oxygen and 92% nitrogen) for 60 min. The hypoxia chamber was partially immersed in warm water to maintain a constant temperature within physiological limits (at 36–37 °C). Following hypoxic exposure, pups were returned to their home cages. Sham operated rats underwent the same surgical procedure. However, they were not subjected to carotid occlusion or to the hypoxic environment (Greggio, De Paula, Azevedo, Venturin, & Dacosta, 2014; Odorcyk, Kolling, Sanches, Wyse, & Netto, 2018).

2.3. ^{18}F-FDG microPET scan

MicroPET scans were conducted at the Preclinical Research Center at the Brain Institute of Rio Grande do Sul (BraIns). Rats underwent imaging examination at PND 60, 53 days post-HI induction, after 12–24 h fasting. The animals were anesthetized individually using a mixture of isoflurane and oxygen (3–4% induction and 2–3% maintenance), and 1 mCi of ^{18}F-FDG was administered intraperitoneally (Zanirati et al., 2018). The animals were returned to the home cage for a 40-minute period of conscious tracer uptake and were placed on a heat plate to maintain the body temperature at 36 ± 1 °C. After the uptake period, the rats were placed in a prone position on the heated bed of the equipment (Triumph microPET, LabPET-4, TriFoil Imaging, Northridge, CA, USA). Static acquisition was conducted under inhaled anesthesia for 10 min with the field of view (FOV: 3.75 cm) centered on the rat's head (Zanirati et al., 2018).

2.4. Image reconstruction and data analysis

An exploratory analysis of glucose metabolism was performed in the whole brain and 24 brain regions bilaterally (auditory, cingulate, entorhinal, frontal, insular, medial prefrontal (MPF), motor, orbitofrontal, parietal, retrosplenial, somatosensory, and visual cortices, nucleus accumbens core shell, amygdala, striatum, hippocampus, olfactory apparatus, hypothalamus, thalamus, superior colliculus, midbrain, ventral tegmental area (VTA), inferior colliculus, and cerebellum). All images were reconstructed using a 3-dimensional maximum likelihood expectation maximization (3D-MLEM) algorithm with 20 iterations. Each reconstructed brain image was spatially normalized using an ^{18}F-FDG brain image template with PMOD 3.5 software and the Fusion toolbox (PMOD Technologies, Zurich, Switzerland). A magnetic resonance imaging (MRI) rat brain voxel of interest (VOI) template was used to overlay the normalized, previously co-rotated images to the microPET imaging database, and 24 VOIs were used. ^{18}F-FDG uptake in whole brain and in all brain regions was normalized by the pons and expressed as relative standardized uptake value (SUVr) (Zanirati et al., 2018).

2.5. Metabolic brain network construction

Regional brain SUVr values were used for metabolic brain network (MBN) analyses. Symmetrical matrices were constructed using 12 VOIs (amygdala, striatum, auditory cortex, entorhinal cortex, insular cortex, parietal cortex, motor cortex, retrosplenial cortex, somatosensory cortex, hippocampus, olfactory apparatus, and thalamus; 24/24 matrices). The MBNs were constructed using Pearson's cross-correlation coefficients and corrected by false discovery ratio (FDR) (Zanirati et al., 2018; Zimmer et al., 2017). These MBNs were bootstrapped (10,000 bootstrap samples) and for each bootstrap sample, the following graph theoretical measures were calculated to compare the networks' matrices: assortativity coefficient, global efficiency, and average clustering coefficient (Rubinov & Sporns, 2010).

2.6. Morris water maze learning task

The Morris water maze (MWM) was used to evaluate spatial memory at PND 65, as described previously (Durán-Carabali et al., 2017; Greggio et al., 2014). The spaced training protocol was performed for 5 successive days. On each day, the rats underwent 4 consecutive training trials and a hidden platform was kept in a constant location in the target quadrant. A different starting location was used in each trial, consisting of a swim followed by a 30-s platform sit. The experimenter guided rats that did not find the platform within 60 s. On the sixth day, a probe trial was performed for memory retention evaluation with the platform absent. The following variables were considered and recorded with ANY-MAZE software (Stoelting Co, Wood Dale, IL, USA): total distance travelled, latency to the previous platform location and time spent in the target quadrant.

2.7. Histological analysis

At PND 70, the animals were euthanized for histological analyses. Rats were anesthetized with a lethal dose of thiopental sodium (100 mg/kg) and subjected to transcardiac perfusion with 0.9% saline solution followed by 4% formaldehyde solution through the left cardiac ventricle. The brains were removed from the skull and kept in formaldehyde solution for at least 24 h, after which the samples were cryoprotected with sucrose solution (30%). Brains were cut on a cryostat into serial 30-μm slices. The cortex, striatum, and hippocampus were identified using the rat brain atlas and the Cavalieri method was used for structural volume measurements as previously described (Alles et al., 2010).

2.8. Statistical analysis

Statistical analysis was performed using PrismGraph 6.0 software (GraphPad Software, San Diego, CA, USA). Data were analyzed using student's *t* test with Welch's corrections or 1-way or 2-way analysis of variance (ANOVA) with Bonferroni correction. Data were expressed as mean and standard deviation (SD) or standard error (SEM) and a significance level of $P < 0.05$ was considered statistically significant for all variables.

Pearson's correlation coefficient was used to assess associations within MBN corrected by false discovery rate (FDR) and between brain ^{18}F-FDG metabolism (SUVr values) and cognitive impairments or brain volume.

3. Results

3.1. Glucose hypometabolism is limited to the ipsilateral brain hemisphere in HI rats at 53 days post-HI insult

For quantification of ^{18}F-FDG brain metabolism, the HI and control animals underwent a microPET-FDG scan at PND 60, corresponding to 53 days after HI brain insult. As Fig. 1A shows, we identified a subtle decrease in whole-brain glucose metabolism for HI animals compared to the sham group ($p = 0.02$). Additionally, we found a significant decrease in brain glucose metabolism limited to the ipsilateral hemisphere in the HI rats ($p = 0.007$, sham $_R$ vs HI $_R$; and $p = 0.005$, HI $_L$ vs HI $_R$; Fig. 1B). There were no differences between the left hemispheres of sham and HI groups or between left and right brain hemispheres in the sham animals. Fig. 1 shows HI rats had reduced right hemisphere ^{18}F-FDG metabolism in the whole cerebral cortex ($p = 0.005$, sham $_R$ vs HI $_R$; and $p = 0.005$, HI $_L$ vs HI $_R$; Fig. 1C), the striatum ($p = 0.0065$, sham $_R$ vs HI $_R$; and $p = 0.0017$, HI $_L$ vs HI R; Fig. 1D), and the hippocampus ($p = 0.005$, sham $_R$ vs HI $_R$; and $p < 0.0001$, HI $_L$ vs HI $_R$; Fig. 1E). There were no differences between sham and HI groups in the contralateral hemisphere for whole brain, whole cortex, striatum, or hippocampus.

When the whole cortex was analyzed, we noted significant hypometabolism in the right hemisphere (Fig. 1). However, when the individual cortices were studied separately, only auditory, entorhinal, insular, parietal, somatosensory, and visual cortices were hypometabolic in the ipsilateral hemisphere, when compared with the same structures on the contralateral side of the brain. Similarly, the glucose metabolism was decreased in the right hemisphere, when compare to sham animals, for the following structures: abc core, amygdala, hypothalamus, superior colliculus, inferior colliculus, and thalamus. There were no changes in ^{18}F-FDG metabolism for cingulate, frontal, MPF, motor, orbitofrontal, retrosplenial, and olfactory cortices, midbrain, VTA, or cerebellum (Supplementary Fig. 1). Additionally, SUVr means ± SDs and p values for all brain regions evaluated are described in Supplementary Tables 1 and 2.

3.2. Intrinsic variability of the Rice-Vannucci model: a significant part of HI animals exhibited no changes to brain glucose metabolism

Furthermore, considering the intrinsic variability of the Rice-Vannucci HI model, an additional analysis was conducted. After the microPET imaging analysis, HI animals were divided into two subgroups at PND 60: HI animals that did not exhibit glucose metabolism changes in the right hippocampus (HI non-hypometabolic: HI non-h group; ^{18}F-FDG-SUVr > or equal 1.19) and animals that did exhibit hypometabolism in the right hippocampus (HI hypometabolic: HI h group; ^{18}F-FDG-SUVr < 1.19). The cutoff criterion was determined based on SUVr calculated for the right hippocampus of adult sham animals (^{18}F-FDG-SUVr mean ± SD = 1.24 ± 0.05). We defined the cutoff value as the mean SUVr minus one SD. Glucose metabolism of the hippocampus ipsilateral to the carotid artery occlusion was used as the cutoff criterion since the hippocampi are widely related to HI pathophysiology leading to cognitive impairments (Alexander, Garbus, Smith, Rosenkrantz, & Fitch, 2014; De Paula et al., 2009; Greggio et al., 2014).

A significant portion of the adult animals subjected to neonatal HI presented a baseline ^{18}F-FDG uptake in the right hippocampus (40.9%, HI non-h group, n = 9/22) similar to sham animals. However, the remaining HI animals (59.1%, HI h group, n = 13/22), exhibited hippocampal hypometabolism according to the cutoff criterion. There was accentuated whole brain hypometabolism in the HI h group compared to both sham and HI non-h groups ($p = 0.0008$ and $p = 0.002$, respectively; Fig. 2B and C). Therefore, the whole brain glucose metabolism reanalysis demonstrated that stratification of HI rats was effective for separating the animals that had marked changes in brain metabolism from those that did not.

Once again, glucose hypometabolism was limited to the ipsilateral brain hemisphere in HI h rats, but not in the HI non-h group, 53 days post-HI insult. Additionally, HI h animals also exhibited glucose hypometabolism in the whole cerebral cortex and striatum ($p < 0.0001$ vs Sham $_R$, HI non-h $_R$, and HI h $_L$; Fig. 2E and F). Detailed values for hippocampus ^{18}F-FDG uptakes can be seen in the Fig. 2G.

Furthermore, in an exploratory analysis of the right brain hemisphere, there was hypometabolism in the auditory, entorhinal, motor, insular, parietal, somatosensory, retrosplenial, and visual cortices. Glucose metabolism in the right hemisphere was also reduced in the abc core, amygdala, hypothalamus, superior colliculus, and thalamus, when compared to the left hemisphere regions of sham, HI non-h, and HI h groups. To a lesser extent, glucose metabolism was also altered in the cingulate cortex, olfactory cortex, VTA, and inferior colliculus. There were no glucose metabolism changes in the frontal, MPF, orbitofrontal, and olfactory cortices, midbrain, or cerebellum (supplementary Fig. 2). For further data, SUVr means ± SDs and p values for all brain regions evaluated are described in Supplementary Tables 3 and 4.

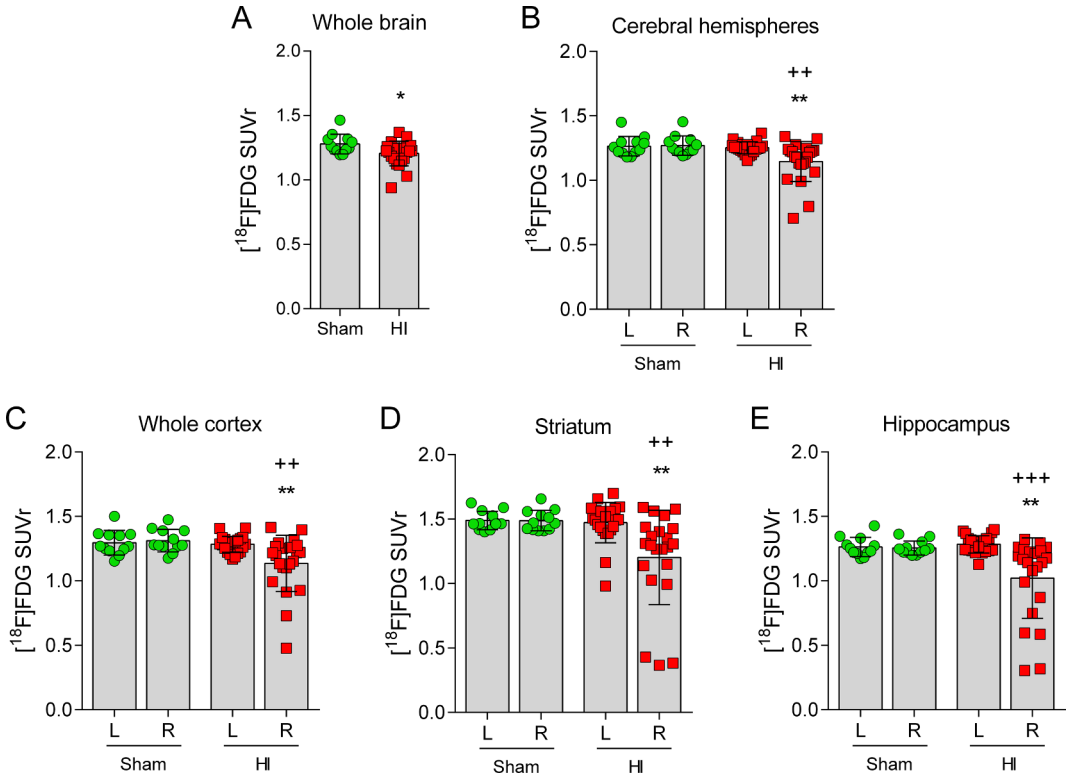

Fig. 1. Changes in whole brain and regional brain glucose metabolism in hypoxic ischemic adult rats. Graphs illustrate changes in ^{18}F-FDG SUVr in sham and HI animals, at PND 60, 53 days post-HI neonatal insult, for the (A) whole brain, (B) cerebral hemispheres, (C) whole cortex, (D) striatum and, (E) hippocampus. * $p < 0.05$ and ** $p < 0.01$ vs sham $_R$ and + + $p < 0.01$ and + + + $p < 0.001$ vs HI $_L$ according to Bonferroni's post hoc after 1-way ANOVA. Data are expressed as mean ± SD, n = 12, sham group and n = 22, HI group. L, left; and R, right.

3.3. The MBN architecture was altered in adult rats previously subjected to neonatal HI

Another important aspect of this study was evaluation of the MBN. The sham group was used to represent an expected MBN (Fig. 3A). Interestingly, HI non-h animals exhibited changes to the MBN architecture, with a substantial decrease in the number of connections compared to the sham group (Fig. 3B). In contrast, HI h animals had increased correlations compared to the HI non-h group. Specifically in the matrix of HI h group, there was a localized increase in positive correlations between regions in the ipsilateral hemisphere and an increase in negative correlations between left and right hemisphere regions (Fig. 3C). Graph theoretical measures revealed consistent reorganization in the MBN in both HI non-h and HI h groups, with lower global efficiency, assortativity coefficient, and average clustering coefficient, compared to the sham group ($p < 0.0001$ vs sham, Fig. 3D, E and F respectively).

3.4. Spatial memory acquisition of adult rats previously subjected to neonatal HI is correlated to brain glucose metabolism

At DPN 65, the animals were tested for spatial memory and learning with the MWM. To evaluate long-term spatial memory, animals underwent training sessions on 5 consecutive days. Throughout all of the learning acquisition sessions, sham animals had superior performance when compared to HI non-h and HI h groups. The mean latency for escape to the platform decreased as training progressed and there was a significant difference between the sham and HI groups from the third day of training sessions until the end of training sessions (3rd-day, $p = 0.0321$ vs HI non-h and $p < 0.0001$ vs HI h; 4th-day, $p = 0.0327$ vs HI non-h and $p < 0.0001$ vs HI h; and 5th-day, $p = 0.0230$ vs HI non-h and $p < 0.0001$ vs HI h; Fig. 4A). In contrast, neither HI group exhibited significant reductions in escape to the platform latency over the following sessions (Fig. 4A). The area under the curve (AUC) of MWM learning acquisition curves demonstrated that HI h and HI non-h groups had poorer performance than sham animals ($p = 0.0294$, sham vs HI non-h; $p < 0.0001$, sham vs HI h; and $p = 0.2540$ HI non-h vs HI h, Fig. 4B). There were no differences between HI h and HI non-h groups in the learning acquisition sessions (Fig. 4B). Additionally, there were no differences between the experimental groups related to the total distance travelled in the probe trial, revealing that there were no limiting motor impairments (Fig. 4C). Both HI h and HI non-h showed increased escape latency ($p = 0.0185$ and $p = 0.0307$, respectively; Fig. 4D) and less time spent in the target quadrant ($p = 0.0297$ and $p = 0.0079$; Fig. 4E) compared to the sham group. Fig. 4F shows a plot illustrating probe trial performance for each experimental group.

The AUC of MWM learning acquisition curves and ^{18}F-FDG uptake values were used to assess whether changes in brain glucose metabolism were correlated with cognitive deficits in HI animals. There were negative correlations between the glucose metabolism and the cognitive impairments for the experimental groups in most of the brain regions evaluated. There were weak negative correlations for the right hemisphere ($r = -0.3757$, $p = 0.028$; Fig. 4G), right cortex ($r = -0.3993$, $p = 0.019$; Fig. 4H), and right hippocampus ($r = -0.3979$, $p = 0.019$; Fig. 4J). In contrast, there was no correlation between right striatum metabolism and cognitive deficits ($r = -0.3011$, $p = 0.083$; Fig. 4I).

In the supplementary analysis, we found moderate negative Pearson correlation coefficients for the following right hemisphere structures: auditory cortex, parietal cortex, retrosplenial cortex, visual cortex, amygdala, hypothalamus, and VTA, and weak negative correlations for the insular cortex, somatosensory cortex, nucleus accubens, superior colliculus, and inferior colliculus (supplementary Fig. 3). There was no correlation between spatial learning ability and glucose metabolism for

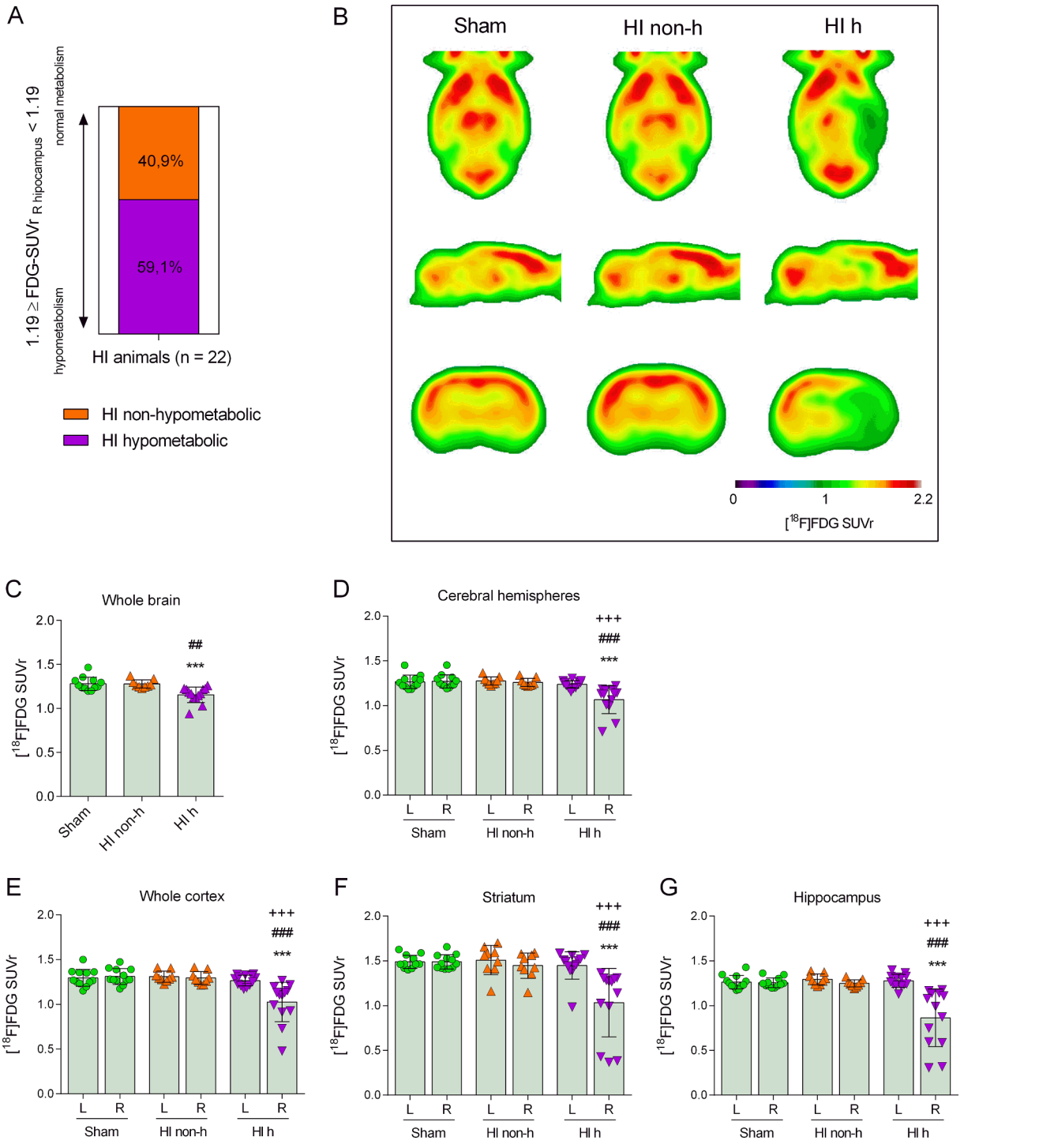

Fig. 2. Brain glucose metabolism variability in adult rats after neonatal HI model. (A) HI animals were divided into two sub-groups based on a sham ^{18}F-FDG SUVr value of R hippocampus into HI non-hypometabolic or HI hypometabolic. (B) The image above shows mean ^{18}F-FDG uptake in the brain for each experimental group (sham, HI non-h, and HI h) at 53 days post-HI induction. ^{18}F-FDG metabolism is illustrated in transverse (top), sagittal (middle), and coronal (bottom) views. Hot colors (shades of red) indicate higher FDG uptake and cold colors (shades of blue) lower uptake. (C) The graphs illustrate brain glucose metabolism differences between groups for the whole brain, (D) cerebral hemispheres, (E) whole cortex, (F) striatum, and (G) hippocampus. * $p < 0.05$, ** $p < 0.01$ and *** $p < 0.001$ vs sham $_R$; # $p < 0.05$, ## $p < 0.01$, and ### $p < 0.001$ vs HI non-h $_R$; and + $p < 0.05$, + + $p < 0.01$ and + + + $p < 0.001$ vs HI h $_L$ according to Bonferroni's post hoc after 1-way ANOVA. Data are expressed as mean ± SD. n = 12 to sham, n = 9 to HI non-hypometabolic, and n = 13 to HI hypometabolic group. HI non-h, HI non-hypometabolic; HI h, hypometabolic; L, left; R, right. (For interpretation of the references to color in this figure legend, the reader is referred to the web version of this article.)

the following right brain regions: cingulate cortex, entorhinal cortex, frontal cortex, MPF cortex, motor cortex, orbitofrontal cortex, olfactory cortex, midbrain, and cerebellum (supplementary Fig. 3).

3.5. Loss of brain volume induced by neonatal HI is restricted to the ipsilateral brain hemisphere and correlates with brain glucose metabolism

Histological brain analysis using the Cavalieri method was

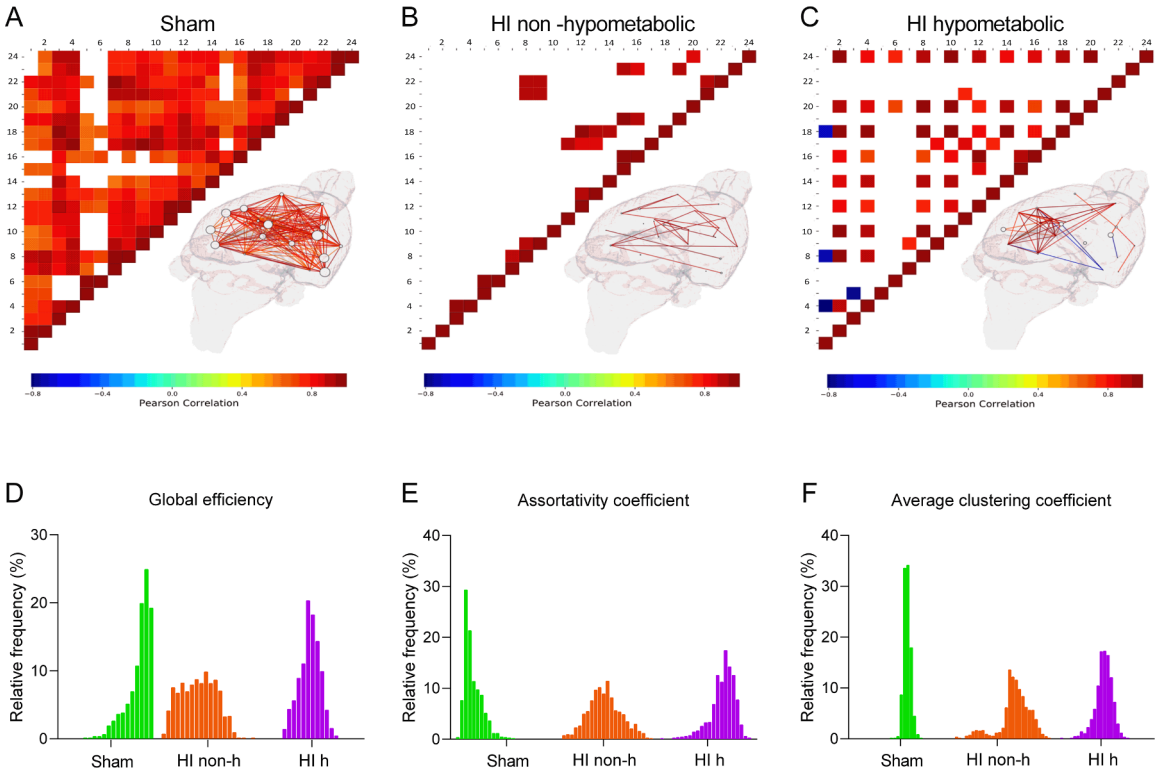

Fig. 3. Alterations in MBN architecture in adult rats previously subjected to the neonatal HI model. (A) Cross-correlation matrices and 3D brain assessed by Pearson correlation representing the brain metabolic network with brain region associations for sham group, (B) HI non-h, and (C) HI-h groups for the following regions: 1- L amygdala, 2- R amygdala, 3- L striatum, 4- R striatum, 5- L auditory cortex, 6- R auditory cortex, 7- L entorhinal cortex, 8- R entorhinal cortex, 9- L insular cortex, 10- R insular cortex, 11- L parietal cortex, 12- R parietal cortex, 13- L motor cortex, 14- R motor cortex, 15- L retrosplenial cortex, 16- R retrosplenial cortex, 17- L somatosensory cortex, 18- R somatosensory cortex 19- L hippocampus, 20- R hippocampus, 21- L olfactory apparatus, 22- R olfactory apparatus, 23- L thalamus, and 24- R thalamus. Hot colors indicate positive correlations (shades of red) and cold colors indicate negative correlations (shades of blue). No correlations are indicated by white color (white = 0). (D) Theoretical graph measures of the metabolic brain network matrices are represented in the graphs related to global efficiency, (E) assortativity coefficient, and (F) average clustering coefficient. n = 12 to sham, n = 9 to HI non-hypometabolic, and n = 13 for HI hypometabolic group. HI non-h, HI non-hypometabolic; and HI h, HI hypometabolic; L, left; R, right. (For interpretation of the references to color in this figure legend, the reader is referred to the web version of this article.)

conducted after microPET-FDG scans and the MWM task. Morphological examination of rat brain slices showed no change in the cerebral hemisphere volumes for any of the experimental groups (Fig. 5A). However, 1-way ANOVA with Bonferroni correction, showed a significant volume decrease in the right hemisphere for the HI h group when compared to sham ($p = 0.010$; Fig. 5A). Regional brain analysis of whole cortex, striatum, and hippocampus showed volume differences between right and left hemisphere only for HI h animals ($p = 0.025$, Fig. 5B; $p < 0.0001$, Fig. 5C; and $p = 0.001$, Fig. 5D respectively). Additionally, there was accentuated brain tissue loss in the right hemisphere volume for these regions in HI h rats in comparison to the sham group ($p = 0.0012$, sham $_{R\ cortex}$ vs HI h $_{R\ cortex}$; $p = 0.0005$, sham $_{R\ striatum}$ vs HI h $_{R\ striatum}$; and $p < 0.0001$, sham $_{R\ hippocampus}$ vs HI h $_{R\ hippocampus}$; Fig. 5B, C, and –D respectively). There were no significant differences in the right and left hemisphere brain volumes or structures for sham or HI non-h groups or between these two groups (Fig. 5A, B, C, and D).

Pearson's correlation coefficient was employed to verify the relationship between brain metabolic changes and loss of brain volume in the HI model. We found moderate positive correlations for all regions evaluated, as follows: right hemisphere ($r = 0.48998$, $p = 0.0038$; Fig. 5E), right cortex ($r = 0.4537$, $p = 0.0080$; Fig. 5F), right striatum ($r = 0.5900$, $p = 0.0003$; Fig. 5G), and right hippocampus ($r = 0.5871$, $p = 0.0003$; Fig. 5H). Fig. 5I shows a visual correlation between brain metabolism and brain tissue volume.

4. Discussion

The aim of the present study was to evaluate *in vivo* changes in the cerebral glucose metabolism and MBN of adult rats after induction of a neonatal HI model. Here, we demonstrated changes in brain glucose metabolism restricted to the hemisphere ipsilateral to carotid artery occlusion. Additionally, confirming the neuroplastic variability of the HI model, we showed that 40.9% of HI rats (HI non-h group) exhibited no changes in brain glucose metabolism or in brain tissue volume by post-mortem histological analysis. However, the remaining 59.1% of HI animals (HI h group) showed a marked brain hypometabolism and reduced brain volume in the ipsilateral hemisphere for most of the brain regions evaluated. Interestingly, all HI animals developed cognitive impairments and showed aberrant MBN architecture in the adult phase after neonatal HI insult.

It is known that some brain regions are more susceptible to HI damage and are widely reported in the pathophysiology of clinical and experimental HI (Batista, Chugani, Juhász, Behen, & Shankaran, 2007; Biran, Verney, & Ferriero, 2012; Kannan & Chugani, 2010; Liu, Siesjö, & Hu, 2004; Vannucci, Lyons, & Vasta, 1988; Wixey, Reinebrant, & Buller, 2011). It has also been shown that glucose metabolism is significantly lower in severe than in mild and medium hypoxic-ischemic neonates (Shi et al., 2012). Batista et al. reported that early transitory hypermetabolism followed by permanent hypometabolism in the striatum and thalamus seems to be related to prognosis of cerebral palsy in newborns affected by HI (Batista et al., 2007). Preclinical studies showed acute and chronically persistent hypometabolism in the

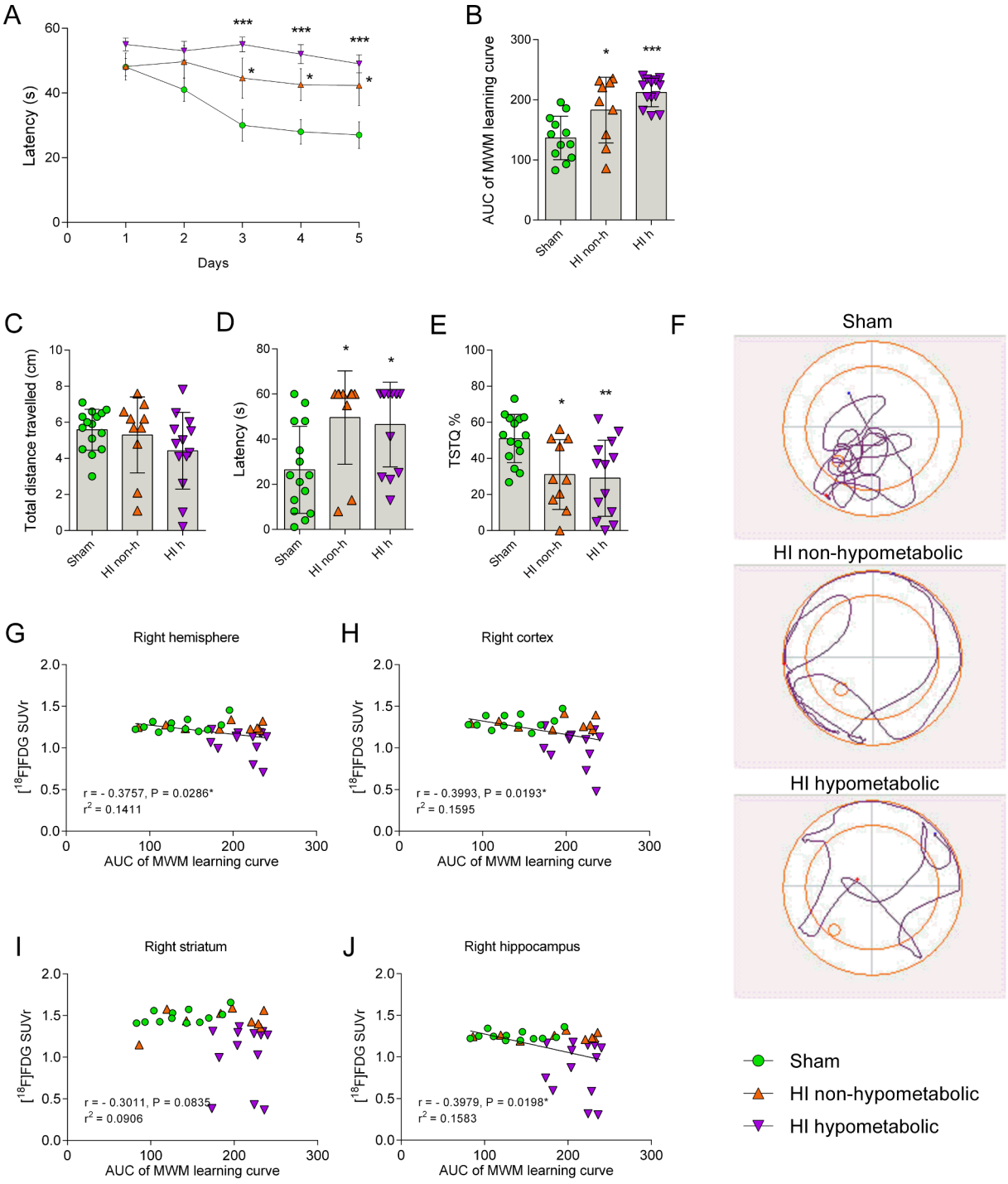

Fig. 4. Long-term cognitive impairments in spatial memory task correlated with the brain glucose metabolism of adult HI rats. (A) The graphs represent the spatial memory acquisition curve and the respective (B) AUC of MWM performance. (C) The following graphs are related to the total distance travelled, (D) the escape latency and, (E) the time spent in the target quadrant in the probe trial. (F) Images show a representative plot of probe performance for each experimental group. * $p < 0.05$, ** $p < 0.01$, and *** $p < 0.001$ vs sham group according to Bonferroni's post hoc test after 2-way and 1-way ANOVA, respectively. Data are expressed as mean ± SD. G) Graphs show Pearson's coefficients for correlations between brain glucose metabolism and AUC of MWM learning curve for R hemisphere, H) R cortex, I) R striatum, and J) R hippocampus. n = 12 to sham, n = 9 to HI non-hypometabolic, and n = 13 to HI hypometabolic groups. HI non-h, HI non-hypometabolic and HI h, hypometabolic.

ipsilateral hemisphere after brain ischemia in adult rats (Gao et al., 2010; Hyun et al., 2011; Li, Lu, & Zhang, 2013). Furthermore, cellular death in the ipsilateral hippocampus has been associated with both necrosis and apoptosis mechanisms in neonatal HI rats (Liu et al., 2004). We did indeed observe accentuated glucose hypometabolism at 53 days after HI insult, in the right hippocampus, right striatum, right thalamus and right auditory, parietal, insular, retrosplenial, somatosensory, and visual cortices. Additionally, we found severe hypometabolism in other structures in the right hemisphere, such as the acb core, amygdala, hypothalamus, superior colliculus, VTA, and inferior colliculus. To a lesser extent, metabolism was also altered in the right cingulate cortex, motor cortex, and midbrain. Nonetheless, no changes

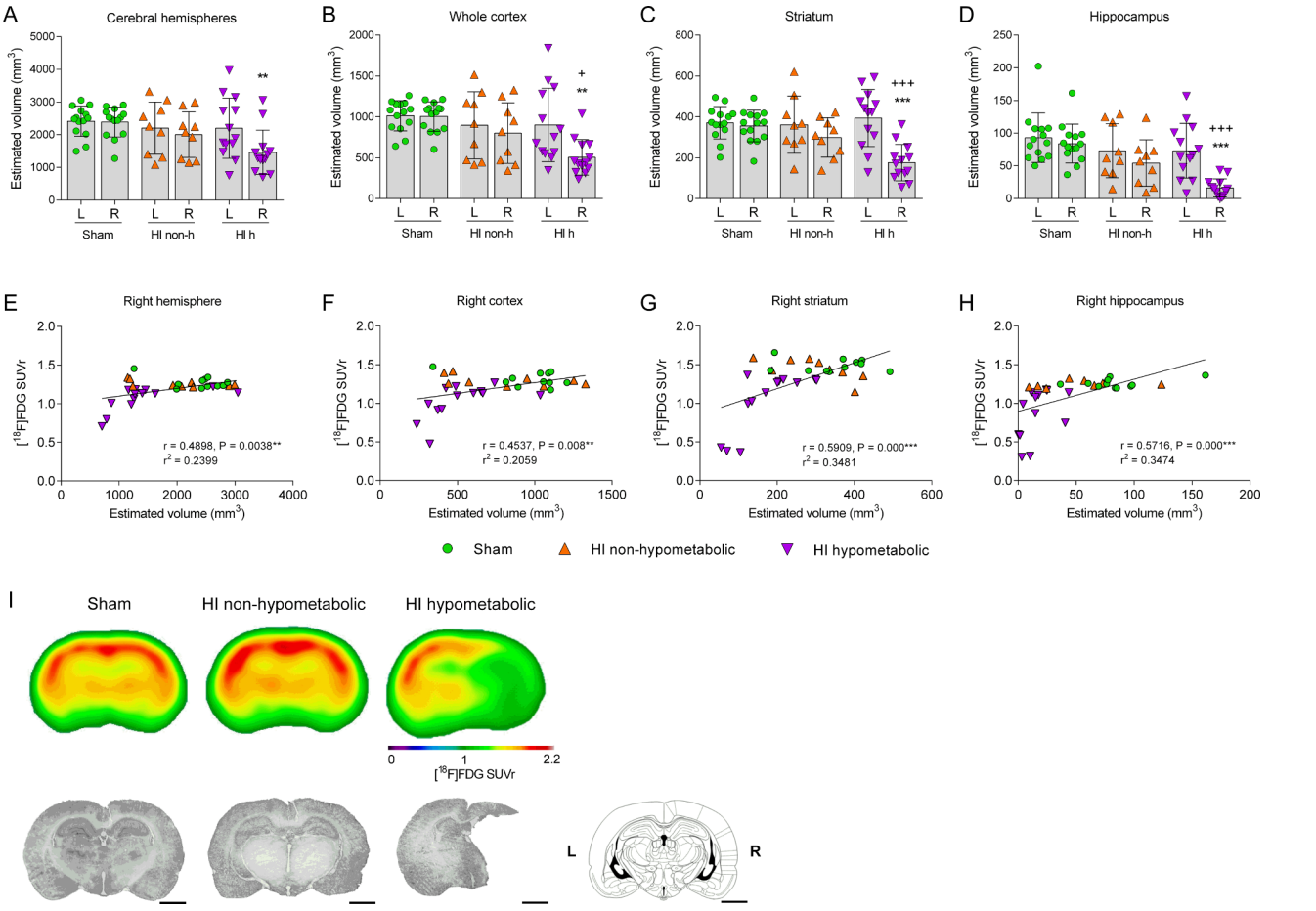

Fig. 5. Brain tissue loss in adult rats after neonatal HI model is correlated with cerebral ^{18}F-FDG metabolism. (A) Estimated brain volumes of the left and right hemispheres, (B) cortex, (C) striatum, and (D) hippocampus. (E) Graphs below show Pearson's coefficients for correlations between brain glucose metabolism and brain volume for hemisphere, (F) cortex, (G) striatum, and (H) hippocampus. ** $p < 0.01$ and *** $p < 0.001$ vs sham $_R$ and + $p < 0.05$, + + $p < 0.01$ and + + + $p < 0.001$ vs HI h $_L$ according to Bonferroni's post hoc test after 1-way ANOVA. (I) Visual representation of brain metabolism correlation with brain volume. The following columns represents FDG-PET scan means from each group and, below, digitalized images of the rat brains corresponding to the coronal sections from sham, HI non-h, and HI-h groups, respectively. The last column shows a correspondent schematic drawing from Paxinos and Watson's atlas. n = 12 to sham, n = 9 to HI non-hypometabolic, and n = 13 to HI hypometabolic groups. HI non-h, HI non-hypometabolic; HI h, hypometabolic; L, left; R, right.

were found in the frontal cortex, MPF cortex, orbitofrontal cortex, or cerebellum. Despite this, in previous studies the frontal cortex has been related with increased neuroinflammation and decreased cerebral blood flow in neonatal HI models (Sizonenko et al., 2003; Vannucci et al., 1988; Wixey et al., 2011). It is possible that the reason that frontal cortices did not exhibit decreased glucose metabolism in the present study is related to their anatomical location, remote from the ischemic area, suffering only the consequences of hypoxia. Hypoxia alone would not be sufficient to cause persistent and significant metabolic changes lasting to adulthood. The cerebellum also appears to be highly susceptible to hypoxic-ischemic damage, because of the vulnerability of Purkinje cells to this condition. Purkinje cell death in the cerebellum was observed at least 20 days after HI brain injury (Biran et al., 2012). However, in the present study, at 53 days after induction of HI brain injury, there was no alteration in cerebellar metabolism.

Additionally, we used microPET analysis to evaluate the MBN of adult HI animals. Functional network associations or dependencies between brain regions indicate neural interactivity and can be measured by EEG, fMRI, or PET, for example. PET-based brain network analysis employs regional variations in metabolic demand in the brain coupling between synaptic activity and energy consumption (reviewed by Choi et al., 2014; Zimmer et al., 2017; Zanirati et al., 2018). In the present study, an interregional cross-correlation method was used for MBN analysis. The regions included in the MBN analysis were selected due to their importance in the pathophysiology of neonatal HI or in agreement with metabolic changes. The sham group showed a typical pattern of a structured MBN, with a large number of connections between the regions evaluated. Interestingly, although there were no changes to *in vivo* brain glucose metabolism for the HI non-h group, these animals did have MBN changes. The MBN exhibited a hyposynchronous pattern with a drastic reduction in connections between regions.

In the HI h group, we identified an increase in aberrant correlations between the regions evaluated, compared to the sham group MBN. There was an increase in positive correlations between right hemisphere regions and a consequent increase in negative correlations between contralateral and ipsilateral brain hemispheres. Specifically, right hemisphere regions correlated positively with each other because of the drastic decrease in their metabolism in synchrony. Conversely, the existence of negative correlations between left and right hemispheres was due to the preserved metabolism in the contralateral hemisphere and intensification of hypometabolism in the injured hemisphere. We therefore demonstrated an MBN with disconnection between the cerebral hemispheres in the HI h animals.

The brain is highly connected by networks and ischemia processes can alter the global brain network (Jung et al., 2016; Siegel et al., 2018). Our study was effective in demonstrating that HI insult changes the architecture of the MBN in adult rats previously subjected to the

neonatal HI model, regardless of presence or absence of significant brain metabolism changes. Based on the premise that synchronic regions are functionally interconnected, the aberrant pattern of synchronization for some HI animals demonstrates the capacity of neonatal HI insult to disrupt the interhemispheric functional connection between brain regions. Siegel et al. also identified specific brain network dysfunction patterns and loss of interhemispheric communication as being associated with impairment of behavioral brain domains in stroke patients (Siegel et al., 2018). Additionally, both HI groups demonstrated a reduction in global efficiency, assortativity coefficient, and average clustering coefficient in the MBN matrix, in relation to the sham group. Decreased global efficiency has been associated with some neurodegenerative pathologies, which indicate loss of efficiency in regional information exchange (Choi et al., 2014; Seo et al., 2013). Indeed, HI h presented an aberrant hypersynchronic pattern whereas HI non-h presented an aberrant hyposynchronic pattern.

Both clinical and experimental studies have linked neonatal HI to unfavorable outcomes for cognitive ability (Alexander et al., 2014; Aylward, 2014; Greggio et al., 2014). The ability to acquire spatial memory is closely related to the functional integrity of both the hippocampus and the striatum (Pooters, Gantois, Vermaercke, & D'Hooge, 2016; Shah, Verhoye, Van der Linden, & D'Hooge, 2018). Controversially, both HI h and HI non-h animals exhibited impaired MWM performance. Even HI animals that did not exhibit hippocampal or striatal changes in either metabolism or morphology showed a significant cognitive impairment compared with the sham group. Additionally, we found a correlation between MWM performance and brain glucose metabolism in most of the regions in the ipsilateral hemisphere, including the right hippocampus but not the right striatum.

In common with the brain metabolism changes, cerebral volume loss was also limited to the ipsilateral hemisphere in the HI h group but not in the HI non-h group. HI animals usually present generalized brain injuries, including volumetric reductions in the ipsilateral cortex, hippocampus, and striatum and increases in ventricular volume associated with persistent behavioral deficits (Alexander et al., 2014; Durán-Carabali et al., 2017; Greggio et al., 2014). However, Smith et al. observed that changes in anatomical volume of different brain regions did not correlate with any behavioral change for HI animals (Smith, Alexander, Chrobak, Rosenkrantz, & Fitch, 2015). In the same manner, we also observed dissociation between cognitive and MBN impairments with an absence of anatomical and metabolic brain changes in the HI non-h animals. Nevertheless, changes in brain volume did correlate positively with the hypometabolism observed in the regions evaluated.

There is consensus that brain ^{18}F-FDG metabolism is proportional to brain energy demand and therefore indicative of synaptic activity (Choi et al., 2014; Zimmer et al., 2017). Furthermore, changes in regional cerebral metabolism are usually associated with brain injuries, such as inflammatory process, cellular death, and tissue loss leading to neurofunctional disabilities (Fu et al., 2009; Love, Tomas, Tronco, & Palestro, 2005; Matsui et al., 2009; Pomykala et al., 2013). As expected, most of the HI animals that exhibited severe hypometabolism in regions of the ipsilateral hemisphere developed cognitive deficits in spatial memory and had significant loss of volume of brain regions. These animals also had altered MBN, with aberrant connections, promoting interhemispheric disconnection. In contrast, we also demonstrated that a percentage of HI animals preserved normal brain glucose metabolism levels and cerebral tissue anatomy. Notwithstanding, they were unable to prevent the development of cognitive deficits caused by neonatal HI insult. These animals also had an abnormal MBN, indicative of changes in brain functionality and possibly related to poor cognitive outcomes. Similarly, patients with epilepsy who present changes to the organization of the cerebral white matter network appear to be sensitive to cognitive decline even without injuries visible on magnetic resonance imaging (Vaessen et al., 2012). In agreement with other studies (Balduini, De Angelis, Mazzoni, & Cimino, 2000; De Paula et al., 2009; Jung et al., 2016), the different degrees of cerebral lesion and outcomes for HI animals observed here may be due to immature brain plasticity providing spontaneous recovery and contributing to anatomical and metabolic maintenance of HI animals. Functional network has dynamic properties and can suffer changes through molecular pathways that do not rely on morphological changes. Similarly, the presence of a structural connection does not prove a functional connection (Biswal et al., 2010). Furthermore, the cognitive impairment seen in the present study was not only related to changes in cerebral integrity, whether morphological or metabolic, but was also related to changes to the conformation of the MBN architecture in HI animals.

5. Summary/Conclusions

In conclusion, our findings show a dissociation between maintenance of brain metabolism and cognitive deficits in the neonatal HI model, which is possibly related to neuroplasticity mechanisms. Absence of changes in brain glucose metabolism, *per se*, were not able to predict adequate cerebral function in HI animals. However, MBN based on microPET-FDG has been shown to be sensitive in revealing changes in brain functionality. Considering the intrinsic variability of HI cerebral damage outcomes, our results highlight an important role for microPET-FDG based MBN in elucidation of whole brain metabolic function in the neonatal HI model. Therefore, the present study demonstrates for the first time that long-term changes in MBN drive memory impairments in adult rats subjected to neonatal hypoxic ischemia, using *in vivo* imaging microPET-FDG.

CRediT authorship contribution statement

Pamella Nunes Azevedo: Conceptualization, Methodology, Validation, Formal analysis, Investigation, Writing - original draft, Visualization, Project administration. **Gabriele Zanirati:** Formal analysis, Validation, Writing - original draft. **Gianina Teribele Venturin:** Formal analysis, Investigation, Writing - review & editing. **Guilherme Garcia Schu:** Formal analysis, Software. **Luz Elena Durán–Carabali:** Investigation, Writing - review & editing. **Felipe Kawa Odorcyk:** Investigation, Writing - review & editing. **Andrey Vinicius Soares:** Investigation. **Gabriela de Oliveira Laguna:** Investigation. **Carlos Alexandre Netto:** Writing - review & editing, Project administration. **Eduardo Rigon Zimmer:** Writing - review & editing, Supervision, Project administration. **Jaderson Costa da Costa:** Writing - review & editing, Supervision, Project administration. **Samuel Greggio:** Conceptualization, Formal analysis, Investigation, Writing - review & editing, Project administration, Funding acquisition.

Declaration of Competing Interest

The authors declare that they have no known competing financial interests or personal relationships that could have appeared to influence the work reported in this paper.

Acknowledgements

This study was financed in part by the Coordenação de Aperfeiçoamento de Pessoal de Nível Superior - Brazil (CAPES; Finance Code 001), and by the Conselho Nacional de Desenvolvimento Científico e Tecnologico - Brazil (CNPq; Chamada Universal MCTI/CNPq N° 01/2016, grant number 405470/2016-9). Other resources were provided by PUCRS (Porto Alegre, Brazil), and Pandurata Alimentos Ltda (São Paulo, Brazil). P. N. Azevedo, and G. Zanirati are recipients of fellowships from CAPES. E. R. Zimmer, C. A. Netto, and J. C. DaCosta are CNPq researchers.

Appendix A. Supplementary material

Supplementary data to this article can be found online at https://doi.org/10.1016/j.nlm.2020.107207.

References

Alexander, M., Garbus, H., Smith, A. L., Rosenkrantz, T. S., & Fitch, R. H. (2014). Behavioral and histological outcomes following neonatal HI injury in a preterm (P3) and term (P7) rodent model. *Behavioural Brain Research*. https://doi.org/10.1016/j.bbr.2013.10.038.

Alles, Y. C. J., Greggio, S., Alles, R. M., Azevedo, P. N., Xavier, L. L., & DaCosta, J. C. (2010). A novel preclinical rodent model of collagenase-induced germinal matrix/intraventricular hemorrhage. *Brain Research, 1356*. https://doi.org/10.1016/j.brainres.2010.07.106.

Aylward, G. P. (2014). Neurodevelopmental outcomes of infants born prematurely. *Journal of Developmental and Behavioral Pediatrics*. https://doi.org/10.1097/01.DBP.0000452240.39511.d4.

Balduini, W., De Angelis, V., Mazzoni, E., & Cimino, M. (2000). Long-lasting behavioral alterations following a hypoxic/ischemic brain injury in neonatal rats. *Brain Research, 859*, 318–325. https://doi.org/10.1016/s0006-8993(00)01997-1.

Batista, C. E. A., Chugani, H. T., Juhász, C., Behen, M. E., & Shankaran, S. (2007). Transient hypermetabolism of the basal ganglia following perinatal hypoxia. *Pediatric Neurology*. https://doi.org/10.1016/j.pediatrneurol.2007.01.004.

Biran, V., Verney, C., & Ferriero, D. M. (2012). Perinatal cerebellar injury in human and animal models. *Neurology Research International*. https://doi.org/10.1155/2012/858929.

Biswal, B. B., Mennes, M., Zuo, X.-N., Gohel, S., Kelly, C., Smith, S. M., ... Milham, M. P. (2010). Toward discovery science of human brain function. *Proceedings of the National Academy of Sciences of the United States of America*. https://doi.org/10.1073/pnas.0911855107.

Brekke, E. M. F., Morken, T. S., Widerøe, M., Håberg, A. K., Brubakk, A. M., & Sonnewald, U. (2014). The pentose phosphate pathway and pyruvate carboxylation after neonatal hypoxic-ischemic brain injury. *Journal of Cerebral Blood Flow & Metabolism*. https://doi.org/10.1038/jcbfm.2014.8.

Choi, H., Kim, Y. K., Kang, H., Lee, H., Im, H. J., Hwang, D. W., ... Lee, D. S. (2014). Abnormal metabolic connectivity in the pilocarpine-induced epilepsy rat model: A multiscale network analysis based on persistent homology. *Neuroimage*. https://doi.org/10.1016/j.neuroimage.2014.05.039.

De Paula, S., Vitola, A. S., Greggio, S., De Paula, D., Mello, P. B., Lubianca, J. M., ... Dacosta, J. C. (2009). Hemispheric brain injury and behavioral deficits induced by severe neonatal hypoxia-ischemia in rats are not attenuated by intravenous administration of human umbilical cord blood cells. *Pediatric Research*. https://doi.org/10.1203/PDR.0b013e31819ed5c8.

Durán-Carabali, L. E., Sanches, E. F., Marques, M. R., Aristimunha, D., Pagnussat, A., & Netto, C. A. (2017). Longer hypoxia–ischemia periods to neonatal rats causes motor impairments and muscular changes. *Neuroscience*. https://doi.org/10.1016/j.neuroscience.2016.10.068.

Fu, Y.-K., Chang, C.-J., Chen, K.-Y., Hwang, L.-C., Wu, K.-H., Chang, K.-W., ... Chang, C.-H. (2009). Imaging of regional metabolic activity by (18)F-FDG/PET in rats with transient cerebral ischemia. *Applied Radiation and Isotopes, 67*, 1743–1747. https://doi.org/10.1016/j.apradiso.2009.03.002.

Gao, F., Wang, S., Guo, Y., Wang, J., Lou, M., Wu, J., ... Zhang, H. (2010). Protective effects of repetitive transcranial magnetic stimulation in a rat model of transient cerebral ischaemia: A microPET study. *European Journal of Nuclear Medicine and Molecular Imaging*. https://doi.org/10.1007/s00259-009-1342-3.

Greggio, S., De Paula, S., Azevedo, P. N., Venturin, G. T., & Dacosta, J. C. (2014). Intra-arterial transplantation of human umbilical cord blood mononuclear cells in neonatal hypoxic-ischemic rats. *Life Sciences*. https://doi.org/10.1016/j.lfs.2013.10.017.

Hyun, H., Lee, J., Hwang, D. W., Kim, S., Hyun, D. K., Choi, J. S., ... Lee, M. (2011). Combinational therapy of ischemic brain stroke by delivery of heme oxygenase-1 gene and dexamethasone. *Biomaterials*. https://doi.org/10.1016/j.biomaterials.2010.08.116.

Johnston, M. V., Fatemi, A., Wilson, M. A., & Northington, F. (2011). Treatment advances in neonatal neuroprotection and neurointensive care. *Lancet Neurology*. https://doi.org/10.1016/S1474-4422(11)70016-3.

Jung, W. B., Im, G. H., Chung, J. J., Ahn, S. Y., Jeon, T. Y., Chang, Y. S., ... Lee, J. H. (2016). Neuroplasticity for spontaneous functional recovery after neonatal hypoxic ischemic brain injury in rats observed by functional MRI and diffusion tensor imaging. *Neuroimage*. https://doi.org/10.1016/j.neuroimage.2015.11.032.

Kannan, S., & Chugani, H. T. (2010). Applications of positron emission tomography in the newborn nursery. *Seminars in Perinatology*. https://doi.org/10.1053/j.semperi.2009.10.004.

Kurinczuk, J. J., White-Koning, M., & Badawi, N. (2010). Epidemiology of neonatal encephalopathy and hypoxic-ischaemic encephalopathy. *Early Human Development*. https://doi.org/10.1016/j.earlhumdev.2010.05.010.

Levine, Seymour (1960). Anoxic-Ischemic Encephalopathy in Rats. *The American Journal of Pathology*.

Li, J. H., Lu, J., & Zhang, H. (2013). Functional recovery after scutellarin treatment in transient cerebral ischemic rats: A pilot study with 18F-fluorodeoxyglucose MicroPET. *Evidence-Based Complementary and Alternative Medicine*. https://doi.org/10.1155/2013/507091.

Liu, C. L., Siesjö, B. K., & Hu, B. R. (2004). Pathogenesis of hippocampal neuronal death after hypoxia-ischemia changes during brain development. *Neuroscience*. https://doi.org/10.1016/j.neuroscience.2004.03.062.

Love, C., Tomas, M. B., Tronco, G. G., & Palestro, C. J. (2005). FDG PET of infection and inflammation. *RadioGraphics*. https://doi.org/10.1148/rg.255045122.

Lubics, A., Reglodi, D., Tamás, A., Kiss, P., Szalai, M., Szalontay, L., & Lengvári, I. (2005). Neurological reflexes and early motor behavior in rats subjected to neonatal hypoxic-ischemic injury. *Behavioural Brain Research*. https://doi.org/10.1016/j.bbr.2004.06.019.

Malisza, K. L., Kozlowski, P., Ning, G., Bascaramurty, S., & Tuor, U. I. (1999). Metabolite changes in neonatal rat brain during and after cerebral hypoxia-ischemia: A magnetic resonance spectroscopic imaging study. *NMR in Biomedicine*. https://doi.org/10.1002/(SICI)1099-1492(199902)12:1<31::AID-NBM544>3.0.CO;2-M.

Matsui, T., Nakata, N., Nagai, S., Nakatani, A., Takahashi, M., Momose, T., ... Koyasu, S. (2009). Inflammatory cytokines and hypoxia contribute to 18F-FDG uptake by cells involved in pannus formation in rheumatoid arthritis. *Journal of Nuclear Medicine*. https://doi.org/10.2967/jnumed.108.060103.

McKenna, M. C., Scafidi, S., & Robertson, C. L. (2015). Metabolic alterations in developing brain after injury: Knowns and unknowns. *Neurochemical Research*. https://doi.org/10.1007/s11064-015-1600-7.

Millar, L. J., Shi, L., Hoerder-Suabedissen, A., & Molnár, Z. (2017). Neonatal hypoxia ischaemia: Mechanisms, models, and therapeutic challenges. *Frontiers in Cellular Neuroscience*. https://doi.org/10.3389/fncel.2017.00078.

Netto, C. A., Sanches, E., Odorcyk, F. K., Duran-Carabali, L. E., & Weis, S. N. (2017). Sex-dependent consequences of neonatal brain hypoxia-ischemia in the rat. *Journal of Neuroscience Research*. https://doi.org/10.1002/jnr.23828.

Odorcyk, F. K., Kolling, J., Sanches, E. F., Wyse, A. T. S., & Netto, C. A. (2018). Experimental neonatal hypoxia ischemia causes long lasting changes of oxidative stress parameters in the hippocampus and the spleen. *Journal of Perinatal Medicine*. https://doi.org/10.1515/jpm-2017-0070.

Pomykala, K. L., Ganz, P. A., Bower, J. E., Kwan, L., Castellon, S. A., Mallam, S., ... Silverman, D. H. S. (2013). The association between pro-inflammatory cytokines, regional cerebral metabolism, and cognitive complaints following adjuvant chemotherapy for breast cancer. *Brain Imaging Behaviour*. https://doi.org/10.1007/s11682-013-9243-2.

Pooters, T., Gantois, I., Vermaercke, B., & D'Hooge, R. (2016). Inability to acquire spatial information and deploy spatial search strategies in mice with lesions in dorsomedial striatum. *Behavioural Brain Research*. https://doi.org/10.1016/j.bbr.2015.11.001.

Rice, J. E., Vannucci, R. C., & Brierley, J. B. (1981). The influence of immaturity on hypoxic-ischemic brain damage in the rat. *Annals of Neurology*. https://doi.org/10.1002/ana.410090206.

Rubinov, M., & Sporns, O. (2010). Complex network measures of brain connectivity: Uses and interpretations. *Neuroimage*. https://doi.org/10.1016/j.neuroimage.2009.10.003.

Sanches, E. F., Arteni, N., Nicola, F., Aristimunha, D., & Netto, C. A. (2015). Sexual dimorphism and brain lateralization impact behavioral and histological outcomes following hypoxia-ischemia in P3 and P7 rats. *Neuroscience*.

Sanches, E. F., Van de Looij, Y., Toulotte, A., da Silva, A. R., Romero, J., & Sizonenko, S. V. (2018). Brain metabolism alterations induced by pregnancy swimming decreases neurological impairments following neonatal hypoxia-ischemia in very immature rats. *Frontiers in Neurology*. https://doi.org/10.3389/fneur.2018.00480.

Seo, E. H., Lee, D. Y., Lee, J. M., Park, J. S., Sohn, B. K., Lee, D. S., ... Woo, J. I. (2013). Whole-brain functional networks in cognitively normal, mild cognitive impairment, and Alzheimer's disease. *PLoS ONE*. https://doi.org/10.1371/journal.pone.0053922.

Shah, D., Verhoye, M., Van der Linden, A., & D'Hooge, R. (2018). Acquisition of spatial search strategies and reversal learning in the Morris water maze depend on disparate brain functional connectivity in mice. *Cerebral Cortex*. https://doi.org/10.1093/cercor/bhy329.

Shankaran, S. (2012). Hypoxic-ischemic encephalopathy and novel strategies for neuroprotection. *Clinics in Perinatology* 10.1016/j.clp.2012.09.008.

Shi, Y., Zhao, J. N., Liu, L., Hu, Z. X., Tang, S. F., Chen, L., & Jin, R. B. (2012). Changes of positron emission tomography in newborn infants at different gestational ages, and neonatal hypoxic-ischemic encephalopathy. *Pediatric Neurology*. https://doi.org/10.1016/j.pediatrneurol.2011.11.005.

Siegel, J. S., Seitzman, B. A., Ramsey, L. E., Ortega, M., Gordon, E. M., Dosenbach, N. U. F., ... Corbetta, M. (2018). Re-emergence of modular brain networks in stroke recovery. *Cortex*. https://doi.org/10.1016/j.cortex.2017.12.019.

Sizonenko, S. V., Sirimanne, E., Mayall, Y., Gluckman, P. D., Inder, T., & Williams, C. (2003). Selective cortical alteration after hypoxic-ischemic injury in the very immature rat brain. *Pediatric Research*. https://doi.org/10.1203/01.PDR.0000072517.01207.87.

Smith, A. L., Alexander, M., Chrobak, J. J., Rosenkrantz, T. S., & Fitch, H. H. (2015). Dissociation in the effects of induced neonatal hypoxia-ischemia on rapid auditory processing and spatial working memory in male rats. *Developmental Neuroscience*. https://doi.org/10.1159/000375487.

Vaessen, M. J., Jansen, J. F. A., Vlooswijk, M. C. G., Hofman, P. A. M., Majoie, H. J. M., Aldenkamp, A. P., & Backes, W. H. (2012). White matter network abnormalities are associated with cognitive decline in chronic epilepsy. *Cerebral Cortex*. https://doi.org/10.1093/cercor/bhr298.

Vannucci, R. C., Lyons, D. T., & Vasta, F. (1988). Regional cerebral blood flow during hypoxia-ischemia in immature rats. *Stroke*. https://doi.org/10.1161/01.STR.19.2.245.

Vial, F., Serriere, S., Barantin, L., Montharu, J., Nadal-Desbarats, L., Pourcelot, L., & Seguin, F. (2004). A newborn piglet study of moderate hypoxic-ischemic brain injury by 1H-MRS and MRI. *Magnetic Resonance Imaging*. https://doi.org/10.1016/j.mri.2004.01.036.

Wixey, J. A., Reinebrant, H. E., & Buller, K. M. (2011). Inhibition of neuroinflammation prevents injury to the serotonergic network after hypoxia-ischemia in the immature

rat brain. *Journal of Neuropathology and Experimental Neurology*. https://doi.org/10.1097/NEN.0b013e3182020b7b.

Zanirati, G., Azevedo, P. N., Venturin, G. T., Greggio, S., Alcará, A. M., Zimmer, E. R., ... DaCosta, J. C. (2018). Depression comorbidity in epileptic rats is related to brain glucose hypometabolism and hypersynchronicity in the metabolic network architecture. *Epilepsia, 59*. https://doi.org/10.1111/epi.14057.

Zimmer, E. R., Parent, M. J., Souza, D. G., Leuzy, A., Lecrux, C., Kim, H.-I., ... Rosa-Neto, P. (2017). [(18)F]FDG PET signal is driven by astroglial glutamate transport. *Nature Neuroscience, 20*, 393–395. https://doi.org/10.1038/nn.4492.